

Fermilab Library



0 1160 0052508 3

SDC-90-00094

SDC
SOLENOIDAL DETECTOR NOTES

INCLUSIVE LEPTON ANALYSIS AT THE Z

J. Frederic Kral

October 5, 1990

MARK II/SLC NOTE #250 AND T/G NOTE #402

AUTHOR: J. Frederic Kral

DATE: October 5, 1990

TITLE: **Inclusive Lepton Analysis at the Z**

This note describes the analysis used to identify leptons at the SLC. Isolated charged tracks identified as electrons or muons are used for the measurement of the Z -boson branching fraction into hadrons containing bottom quarks [Kral 90a]. This note is adapted from Chapter 5 of my thesis [Kral 90b].

The note preceding this one, Mark II/SLC Note #249, *SLC Lepton Identification Software* [Kral 90c], is a users' guide to the SLC software, as embodied in my two subroutines [ECPUB 192] SLCELECFORTRAN and [ECPUB 192] SLCMUONFORTRAN, where [ECPUB 192] is the Mark II G disk on SLACVM.

Together, these two notes (#249 and #250) supercede but do not entirely replace the unofficial memos, *Muon Identification Using the Muon System at the SLC* [Kral 89a] and *Electron Identification Using the LA Calorimeter at the SLC* [Kral 89b], circulated during October 1989.

The following sections describe the isolation criterion for charged tracks reconstructed in the central drift chamber and the methods for identifying leptons. Electrons are identified as tracks with large energy-deposits in the front of the liquid argon barrel calorimeters and muons are identified as tracks which penetrate through the hadron absorber to the outer layers of the muon system. First for electrons and then for muons, we calculate the probability for an isolated lepton track to be identified as a lepton, the probability for an isolated hadron track to be misidentified as a lepton, and the errors on these probabilities, used in the determination of the efficiency for tagging $b\bar{b}$ events. The note is divided into the following sections and appendix,

1. Track Isolation Criterion
2. Electron Identification
3. Muon Identification
4. Acknowledgments
- A. Muon Monte Carlo Corrections.

1. Track Isolation Criterion

We define the track isolation criterion to separate $b\bar{b}$ events from $udsc$ events. Because of the larger rest mass of the b quark as compared to $udsc$ quark masses, leptons from semileptonic B hadron decays receive larger momenta in the parent hadron rest frame than those from decays of hadrons containing the lighter quarks. This results in larger momenta transverse to the direction of the parent hadron for leptons in b jets than for leptons in $udsc$ jets.

To determine transverse momenta, we approximate the directions of the parent b quarks with the directions of the hadronic jets. In the analysis done at $E_{\text{cm}} = 29$ GeV [Nelson 83a], the jet directions were defined to be along the direction of the thrust axis. Because the jets are more collimated and the strong coupling constant is smaller, the angular error introduced by reconstructing the parent hadron direction is smaller at 91 GeV than at 29 GeV, as can be seen in the second and third columns of Table 1.

Events	Thrust axis		Nearest cluster	
	29 GeV	91 GeV	29 GeV	91 GeV
$udscb$	20°	14°	11°	6°
$b\bar{b}$	14°	11°	11°	5°
2-jet	13°	7°	11°	6°

Table 1: Average angle between the reconstructed jet direction and the parent hadron direction. The jet direction is estimated by either the thrust axis or the nearest cluster for simulated events for $E_{\text{cm}} = 29$ GeV and for $E_{\text{cm}} = 91$ GeV. The events labelled ‘2-jet’ are events for which the Lund cluster algorithm found two clusters.

However, at 91 GeV, the lepton momenta are larger by about a factor of three compared to those at 29 GeV, and the effect of these angular errors on the transverse momenta becomes significant. To reduce these errors, instead of using the thrust axis, we use the Lund cluster algorithm [Sjöstrand 83] to find the jet directions from the momentum vectors of the charged and neutral particles in each event. When the jet resolution parameter is set equal to its default value, $d_{\text{join}} = 2.5$, we observe an average jet multiplicity of 3.0, with 21% of the detected hadronic events having 4 or more jets. The last two columns of Table 1 show that the added degrees of freedom, obtained from using clusters rather than the thrust axis to reconstruct the jet directions, substantially reduce the errors in estimating the parent hadron direction.

We then define the transverse momentum of each track with respect to the nearest cluster formed by the other charged and neutral particles in the event, $p_t = p \sin \theta_j$, where θ_j is the angle between the track and the cluster (j) closest to the track. To separate leptons that are products of bottom-hadron decay from leptons that are products of primary charm-hadron decay, we choose a cut in p_t from the spectra of Figure 1. We call a track isolated if it has

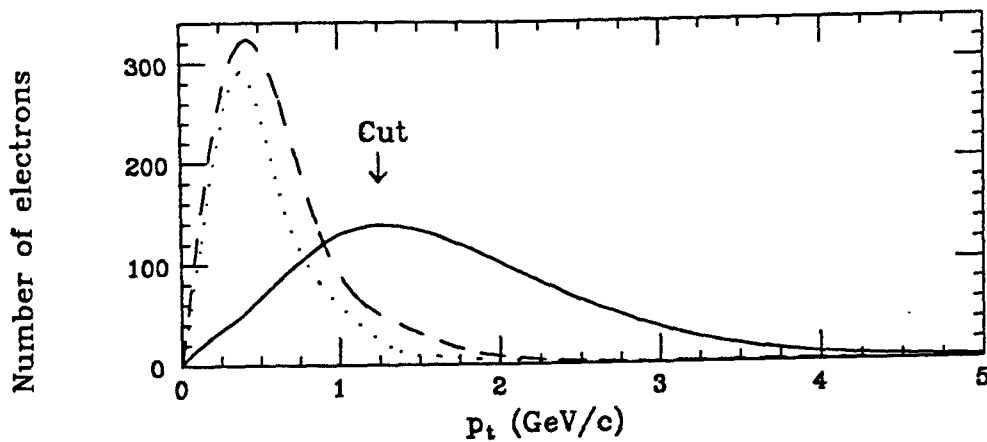


Figure 1: Transverse momentum spectra of Monte Carlo-generated electrons from primary bottom-hadron decay (solid line), secondary bottom-hadron decay (dashes) and primary charm-hadron decay (dots). We define isolated electrons to have $p_t > 1.25$ GeV/ c .

$p_t > 1.25$ GeV/ c .

For electron and muon identification, we consider isolated reconstructed charged tracks which have momenta greater than 2 GeV/ c and which point from the DC to either the LA calorimeter or the muon system.* The p_t distribution of all tracks with $p > 2$ GeV/ c pointing to the LA or muon systems in the data is compared with predictions from the two Monte Carlo models[†] in Figure 2. Because the amount of data is insufficient to distinguish between the models, we use the average of the two models as the prediction to be compared with data, and the difference between the two models as the estimate of the systematic error due to model dependence.

2. Electron Identification

To obtain a pure sample of electrons, we need to efficiently identify electrons while rejecting hadrons. Separation is possible since electrons lose energy differently from other stable charged particles while passing through matter. Our method is adapted from the procedures developed for electron identification with the LA calorimeter at PEP [Nelson 83a, Nelson 83b].

*The minimum momentum required for a muon to penetrate to the outer layer of the muon system at normal incidence is about 1.8 GeV/ c .

[†]The Monte Carlo simulations, based on the parton-shower models BIGWIG 4.1 with Webber cluster fragmentation [Marchesini 84, Webber 84] and JETSET 6.3 shower with Lund string fragmentation [Sjöstrand 86, Sjöstrand 87, Bengtsson 87], are described in the previous note (# 249) [Kral 90c] and in Chapter 3 of my thesis [Kral 90b].

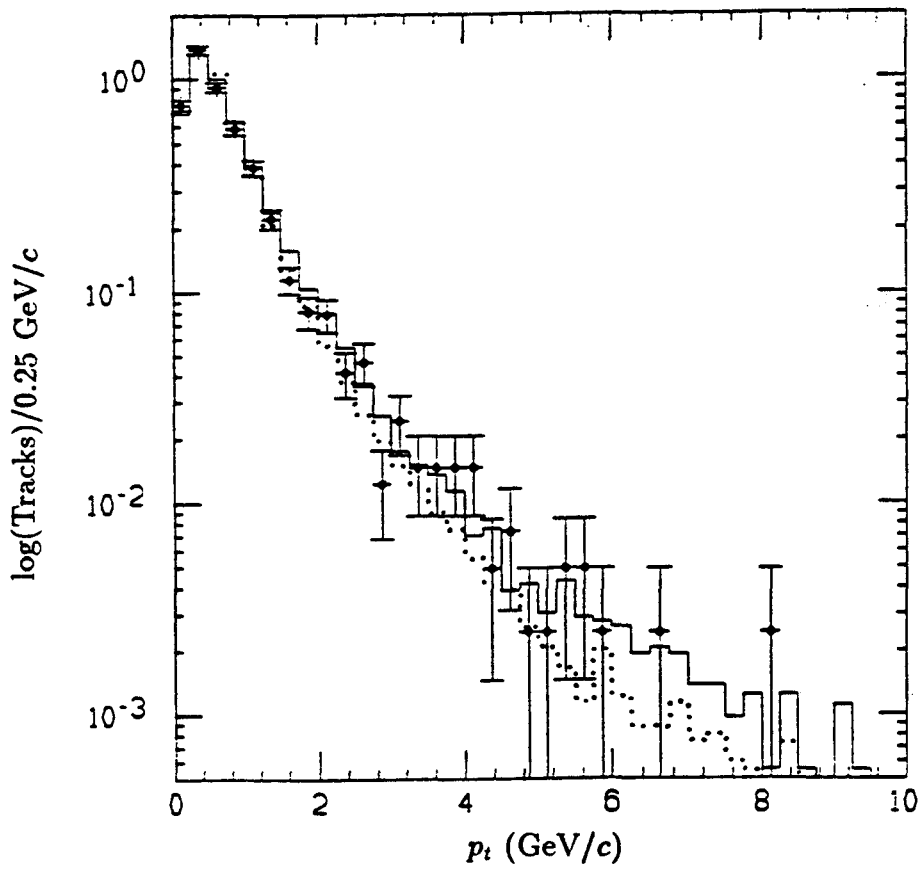


Figure 2: The p_t spectra of tracks with $p > 2$ GeV/c pointing to the LA or muon systems in the data (circles), the Webber-Marchesini model (solid), and the Lund model (dots). Isolated tracks considered for lepton identification have $p_t > 1.25$ GeV/c.

2.1 Method for Identifying Electrons

Electrons above the critical energy, 7 MeV in lead, lose energy principally by bremsstrahlung, radiating photons which in turn interact with matter to either create electron-positron pairs or to eject single electrons from atoms via Compton scattering. The result is an electromagnetic cascade shower. The length of such a shower is related to the radiation length in the absorber, namely 0.56 cm in lead. The energy lost through bremsstrahlung is inversely proportional to the square of the mass of the particle; hence, little energy is lost through this process for charged particles heavier than the electron. Instead, hadrons lose their energy by nuclear interactions, producing hadronic showers with a longitudinal extent related to the nuclear interaction length, namely 17 cm in lead.

To distinguish between electrons and hadrons, the electron identification algorithm uses the fact that hadronic showers are spatially much more extended than electromagnetic showers. Electrons are identified by requiring that a large fraction of their energy, as determined from the momentum measurement in the DC, is deposited in the front half (seven radiation lengths) of the LA calorimeter. This requirement works well for identifying single electrons, but leads to too many hadrons misidentified as electrons in hadronic jets. Misidentification in jets comes largely from overlap of charged particles with electromagnetic deposits from photons, most of which are decay products of neutral pions. To reduce this background from overlapping neutral deposits, we require large energy-deposits in narrow roads around the DC track extrapolation in all three orientations of strips in the front section of the calorimeter.

After a discussion of the calibration of the electron identification algorithm, we calculate the identification efficiency and misidentification probability for isolated tracks in hadronic Z decays.

2.2 Calibration of the Electron Algorithm

We calibrate the identification algorithm on known electrons from radiative and non-radiative Bhabha scattering, recorded in the upgraded Mark II detector at the PEP storage ring. For each track, we calculate $r_i = E_i/p$, where E_i is the energy deposited in a particular strip orientation of the front half of the calorimeter and $i = 1-3$ represents the readout layers F1+F2, T1 and U (which measure the ϕ , θ and u coordinates). The energies E_i are calculated by adding the energies deposited in a narrow road around the DC track extrapolation. The width of the road is calculated from the formula

$$w_{\text{road}} = w_{\text{shower}} + w_{\text{gang}} |\tan(\psi)|, \quad (1)$$

where w_{shower} represents the typical width of an electromagnetic shower ($\simeq 3$ cm), w_{gang} reflects the additional width arising from the separation of the front and back of a ganged layer ($\simeq 4-7$ cm), and ψ is the angle, between the track extrapolation and the normal of the layer, projected onto the plane perpendicular to the orientation of the strips.[†] To reduce

[†]We use $|\tan(\psi)| = |\tan(\phi - \frac{\pi}{4}m + \frac{\pi}{8})|$, $|\tan(\theta - \frac{\pi}{2})|$ and $|\tan(\phi - \frac{\pi}{4}m + \frac{\pi}{8}) - \tan(\theta - \frac{\pi}{2})|$ for the respective layers F, T and U, where $m = 1-8$ is the LA cryostat module number.

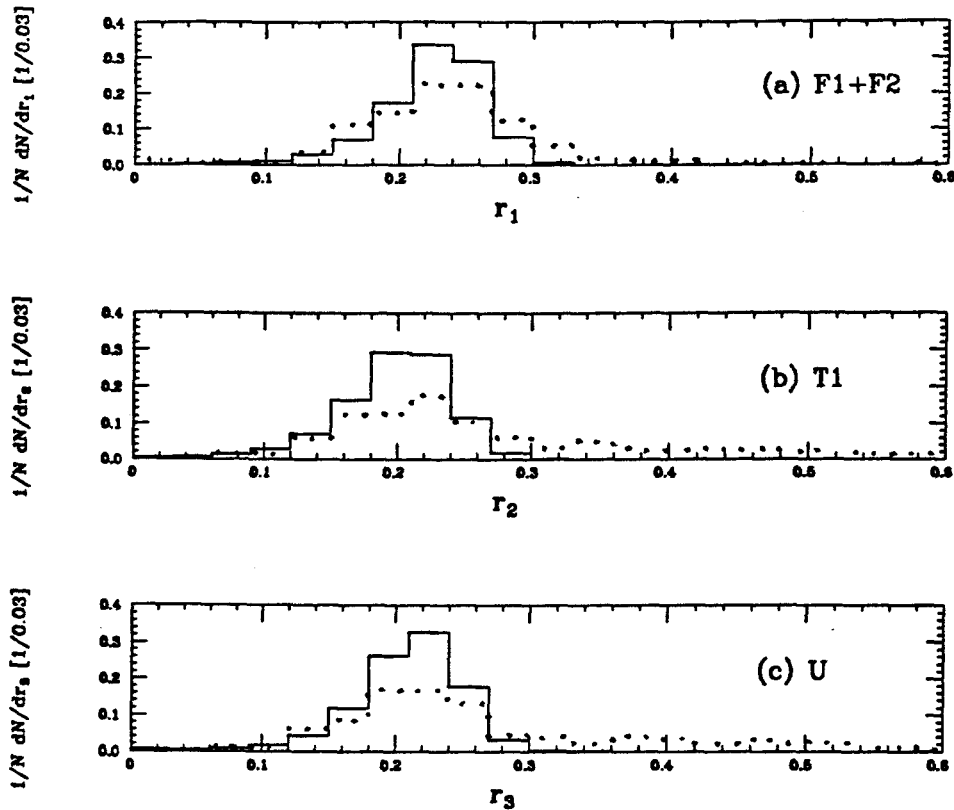


Figure 3: The ratios E/p in the layers (a) F1+F2, (b) T1 and (c) U for Bhabha electrons with $13 < p < 16$ GeV/c (solid) and radiative Bhabha electrons with $3 < p < 8$ GeV/c (dots) recorded with the upgraded Mark II detector at PEP.

misidentification from overlap in the denser jets at the SLC, we have narrowed w_{gang} by a factor 0.6 from the values used at PEP, leading to the widths in Table 2. The resulting

Layer	w_{shower}	w_{gang}	Strip width
F1, F2	0.75	0.5	3.5 cm
T1	0.75	0.9	3.5 cm
U	0.70	0.9	5.4 cm

Table 2: Values used to define w_{road} in units of strip width.

distributions of r_i for the Bhabha electrons are shown in Figure 3.

The electron identification criteria are defined with respect to the median values of r_i and $\sum r_i$ for the calibration electrons, since these medians represent typical electron signals. The medians of the r_i distributions and of $\sum r_i$ are given for three different momentum ranges in Table 3. We require each value r_i to be at least 55% of the median value for the calibration

p range (GeV/c)	r_1 (F1+F2)	r_2 (T1)	r_3 (U)	$\sum r_i$ (F1+F2+T1+U)
3-8	0.235	0.235	0.235	0.725
8-13	0.235	0.210	0.220	0.665
13-16	0.230	0.205	0.215	0.645

Table 3: Median r_i and $\sum r_i$ for radiative ($p < 13$ GeV/c) and non-radiative ($p > 13$ GeV/c) Bhabha electrons at PEP used in defining electron identification cuts.

electrons and $\sum r_i$ to be at least 65% of the median value for the sum.[§] These requirements can be concisely stated as $r_{\min} > 0.55$ and $r_{\text{sum}} > 0.65$, where $r_{\min} = \min(r_i/\text{median } r_i)$ and $r_{\text{sum}} = (\sum r_i/\text{median } \sum r_i)$ are shown in Figure 4.

2.3 Electron Identification Efficiency

A large fraction of tracks in hadronic events fail electron identification by failing the LA fiducial criterion, that the DC track extrapolation be contained within 1.5 units of strip width from the edges of the F1, F2 and T1 layers. This criterion is well-simulated in the Monte Carlo: the fraction of reconstructed tracks[¶] with $p > 2$ GeV/c which are inside the LA fiducial volume is 0.726 ± 0.001 in the MC and 0.74 ± 0.01 in the data.

The efficiency for identifying isolated electron tracks pointing to the LA in hadronic events is 0.83 ± 0.05 , as calculated from the numbers of isolated MC electron tracks in Table 4.

Particle	Webber-Marchesini	Lund	Both models
Electron	388/465 = 0.834	292/356 = 0.820	680/821 = 0.828 ± 0.014
Non-electron	91/13192 = 0.0069	76/10709 = 0.0071	167/23901 = 0.0070 ± 0.0006

Table 4: The numbers of isolated electron and non-electron tracks identified as electrons in the Monte Carlo. The denominators are the numbers of tracks with $p > 2$ GeV/c and $p_t > 1.25$ GeV/c which point to the LA fiducial volume, and the numerators are the subsets of these tracks which satisfy $r_{\min} > 0.55$ and $r_{\text{sum}} > 0.65$. The statistical errors for ratios of numbers, shown here and elsewhere in this note, are obtained from the binomial distribution [James 80].

[§]For tracks with $p < 3$ GeV/c or with $p > 16$ GeV/c, we use the normalization constants from the 3 GeV/c $< p < 8$ GeV/c or 13 GeV/c $< p < 16$ GeV/c ranges, respectively.

[¶]Reconstructed tracks satisfy $|\cos \theta| < 0.85$.

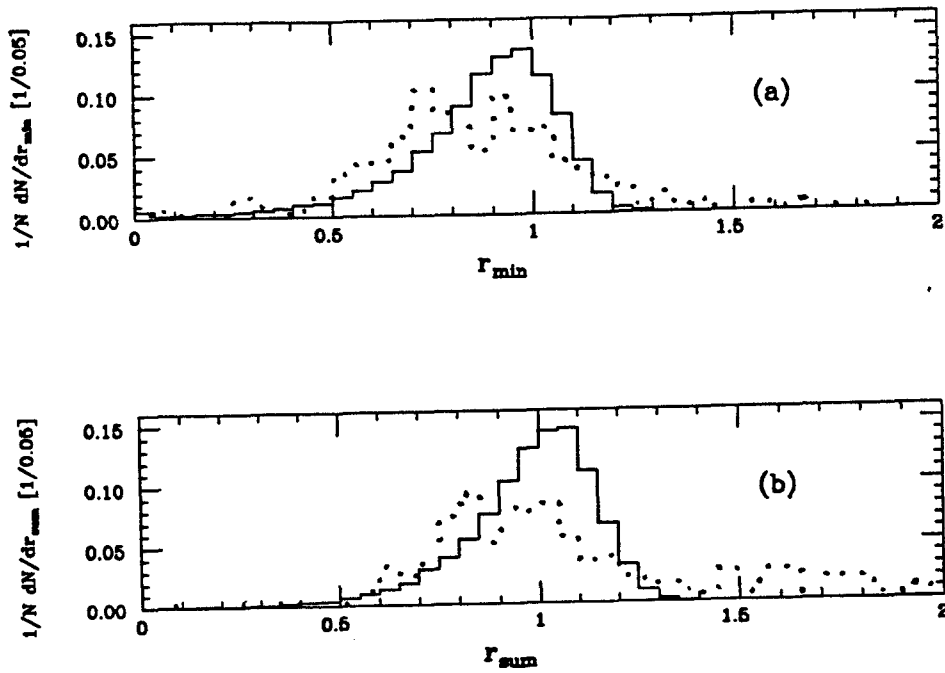


Figure 4: Distributions of (a) r_{\min} and (b) r_{sum} for Bhabha electrons with $13 < p < 16 \text{ GeV}/c$ (solid) and radiative Bhabha electrons with $3 < p < 8 \text{ GeV}/c$ (dots) recorded with the upgraded Mark II detector at PEP. Identified electrons satisfy $r_{\min} > 0.55$ and $r_{\text{sum}} > 0.65$.

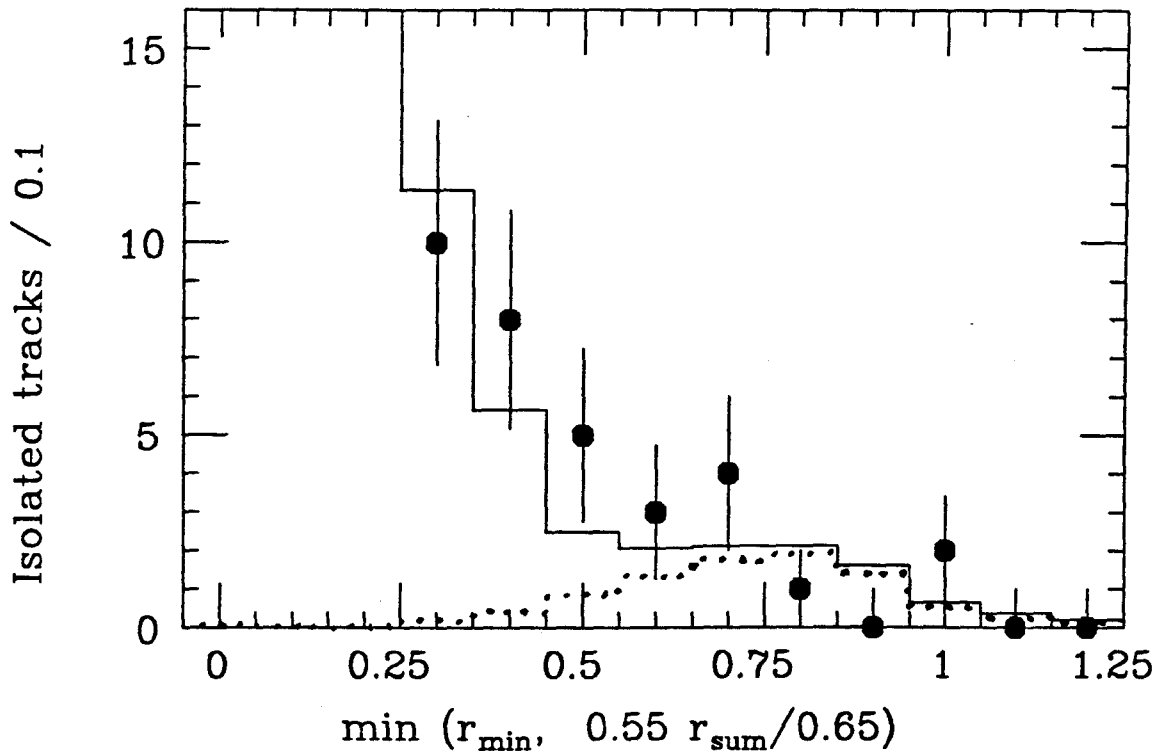


Figure 5: Comparison of electron identification variable in the data (circles) and the MC (solid) for isolated tracks. The dotted histogram is the prediction for real electrons. Identified electrons have $\min(r_{\min}, 0.55r_{\text{sum}}/0.65) > 0.55$.

2.4 Electron Misidentification Probability

The main source of contamination of the electron sample is a combination of interacting hadrons and overlapping neutral deposits. We represent this background in the MC hadronic events by combining signals from pions in tau-pair events recorded at PEP with simulations of electron-photon cascades (EGS4) [Nelson 85]. Figure 5 is a comparison between the cut in the identification variables r_{\min} and r_{sum} for isolated tracks in the data and in the MC, indicating the predicted contribution from real electrons.

We calculate the probability for isolated non-electron tracks to be misidentified as electrons to be 0.007 ± 0.004 from the numbers of isolated MC non-electron tracks in Table 4.

The p_t spectrum for tracks identified as electrons is shown in Figure 6, together with predictions for the contributions from real electrons and hadrons misidentified as electrons. There are 10 isolated tracks identified as electrons in the data, two of which are in the same event. Of these 10 tracks, 2.0 are expected to come from hadrons misidentified as electrons. Figure 7 is a picture of an event with an isolated electron.

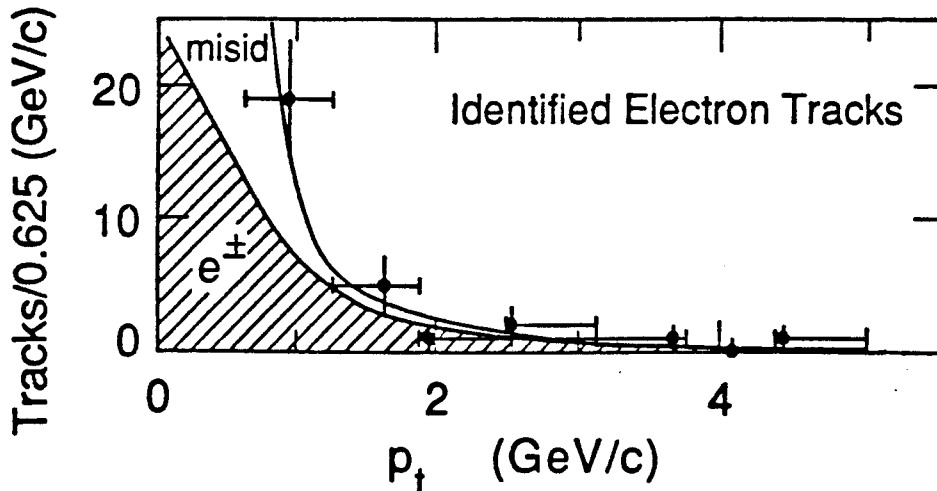


Figure 6: The p_t spectrum for tracks identified as electrons. The shaded and unshaded regions show the expected contributions from real electrons and hadrons misidentified as electrons, respectively. The predictions come from MC simulations normalized to 413 observed hadronic events, assuming $r_b = 0.22$. Isolated electron tracks have $p_t > 1.25$ GeV/c.

3. Muon Identification

To obtain a pure sample of muons, we need to efficiently identify muons while rejecting hadrons. Separation is possible since muons penetrate matter further than other stable charged particles. Our method is adapted from the procedures developed for muon identification with the muon system at PEP [Nelson 83b, Ong 88].

3.1 Method for Identifying Muons

Muons with energies above a few hundred MeV experience energy loss, dE/dx , by ionizing atoms and molecules in a material at an approximately uniform rate, which is 12 MeV/cm in iron. Since the relatively large mass of the muon suppresses bremsstrahlung, muons do not deposit their energy in electron-photon showers like electrons do. Although both muons and charged hadrons undergo similar dE/dx losses, only charged hadrons lose energy through nuclear interactions, since muons do not interact strongly. The nuclear interaction length in iron is the same as in lead, 17 cm. Thus, while 2-GeV muons penetrate more than seven interaction lengths of iron, most charged hadrons are absorbed in this amount of iron, in which they produce hadronic showers.

To distinguish between muons and hadrons, the muon identification algorithm uses the fact that while muons penetrate matter, hadrons produce showers in matter. Muons are identified as tracks which penetrate through the seven interaction lengths of absorber, leaving hits in all four layers of the muon system. Misidentification comes from hadron punch

RUN 19094 REC 004 E= 91.09 11 PRONG HADRON
 TRIGGER 0 4CF CHAR SST CTF

(5-0)
 MARK 11 AT SLC

TRK	P	ELATOT	ID
1	4.1		PI ⁺
2	1.2	0.7	P ⁻
3	0.3	0.2	PI ⁻
4	1.6		PI ⁻
5	6.2	0.3	PI ⁻
6	0.7		PI ⁺
7	7.4		PI ⁺
8	0.2		PI ⁺
9	1.8	1.4	PI ⁺
10	7.1	4.8	E ⁻
11	3.8		PI ⁻
12	3.8		PI ⁻
13		0.1	G
14		0.2	G
15		1.4	G
16		0.6	G
17		1.0	G
18		1.1	G
19		0.6	G
20		1.2	G
21		0.9	G
22		0.4	G
23		1.8	G
24		2.1	G
25		0.2	G
26		0.6	G
27		13.1	G
28		0.2	G
29		0.3	G
30		0.5	G
31		0.2	G
32		0.4	G

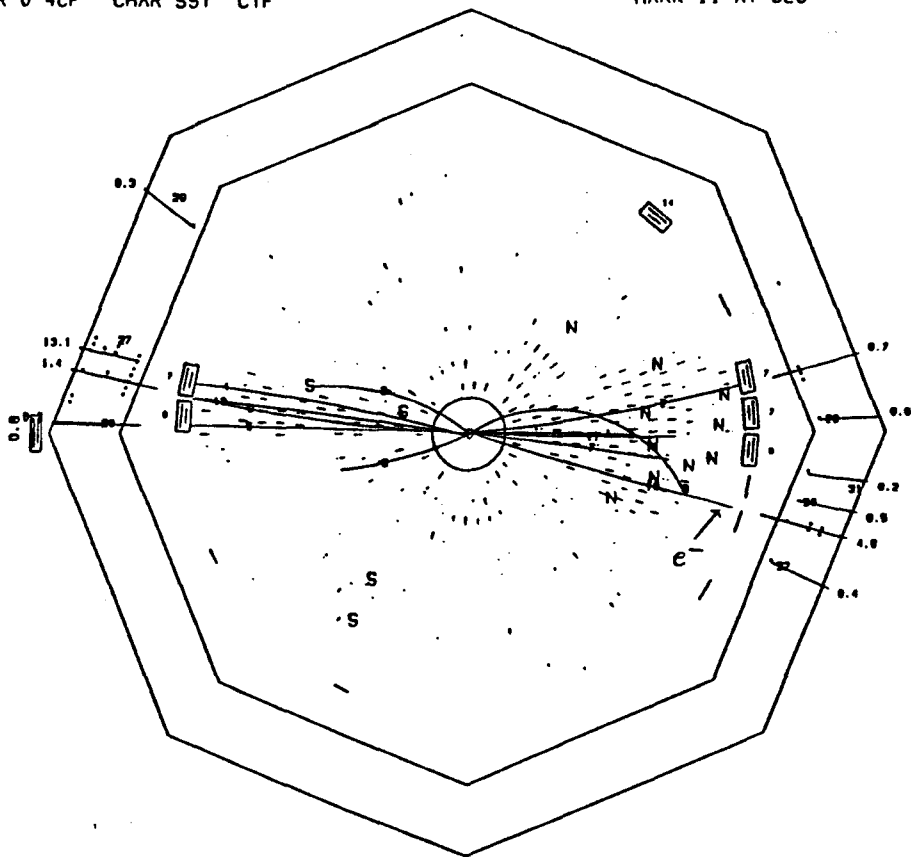


Figure 7: Hadronic Z -decay event with an isolated electron shown with charged tracks and neutral showers in the r - ϕ plane. Track number 10 has $p = 7.1$ GeV/ c , $p_t = 1.5$ GeV/ c , $r_{\min} = 0.73$ and $r_{\text{sum}} = 0.75$.

through, track overlap and noise hits. Requiring that each of the hits be located near the DC track extrapolation greatly reduces these backgrounds. We also require correlated hits in the outer three layers of the muon system, thereby further reducing misidentification from beam-induced noise in these layers.

After a discussion of the calibration of the muon identification algorithm, we calculate the identification efficiency and misidentification probability for isolated tracks in hadronic Z decays.

3.2 Calibration of the Muon Algorithm

We calibrate the identification algorithm on known muons from cosmic-ray events and on muon-pair events recorded in the upgraded Mark II detector at the PEP storage ring. For each track, we look for hits in the muon-chamber proportional tubes within a search region around the DC track extrapolation. The search region width is 3σ , where σ is the rms error of track extrapolation.^{||}

We use $\sigma^2 = \sigma_{\text{scatt}}^2 + \sigma_{\text{res}}^2$, where σ_{scatt} is the error due to multiple Coulomb scattering and σ_{res} is the combined resolution of the muon chambers and the DC tracking. The amount of multiple Coulomb scattering for a particle incident on a piece of material in the detector depends on the particle momentum as well as the material thickness. The rms scattering angle is approximated as

$$\Theta = \frac{21\text{MeV}/c}{p\beta} \sqrt{\frac{t}{X_0}}, \quad (2)$$

where β is the velocity of the incident particle, t is the thickness of the material and X_0 is its radiation length. The multiple-scattering contributions due to each of the detector elements, the magnet coil ($1.3X_0$), the LA calorimeter ($15X_0$) and the hadron absorbers ($14\text{--}18X_0/\text{layer}$), are added in quadrature. The error in the measured coordinate is

$$\sigma_{\text{scatt}}^2 = \frac{1}{2} \sum_i \Theta_i^2 \left(\frac{t_i^2}{3} + t_i d_i + d_i^2 \right), \quad (3)$$

where d_i is the distance following element i to the given layer and the factor $1/2$ arises from projecting Θ onto a plane. The typical position error for a 2-GeV muon due to multiple scattering is 5 cm at the first layer of the muon system and 10 cm at the fourth layer.

We use cosmic rays, recorded with the Mark II at the SLC, to calculate the error at each layer due to the resolution of the muon chambers (about $2.5 \text{ cm}/\sqrt{12} = 0.7 \text{ cm}$) and the DC track extrapolation. These resolution errors are smaller than at PEP, due to the superior drift chamber at the SLC, especially in the z coordinate. Figure 8 shows the distance between the track extrapolation and the nearest hit, divided by σ , for cosmic-ray muons.

^{||}In the analyses done at PEP [Nelson 83b, Ong 88], the search region was defined to be 2σ . Our wider region (3σ) is less sensitive to misalignments. The beam-induced noise levels in the outer layers of the muon system are much higher at the SLC than at PEP. To better reject noise hits in layers 2–4, we have added the requirement that these hits be correlated, as is explained on page 14.

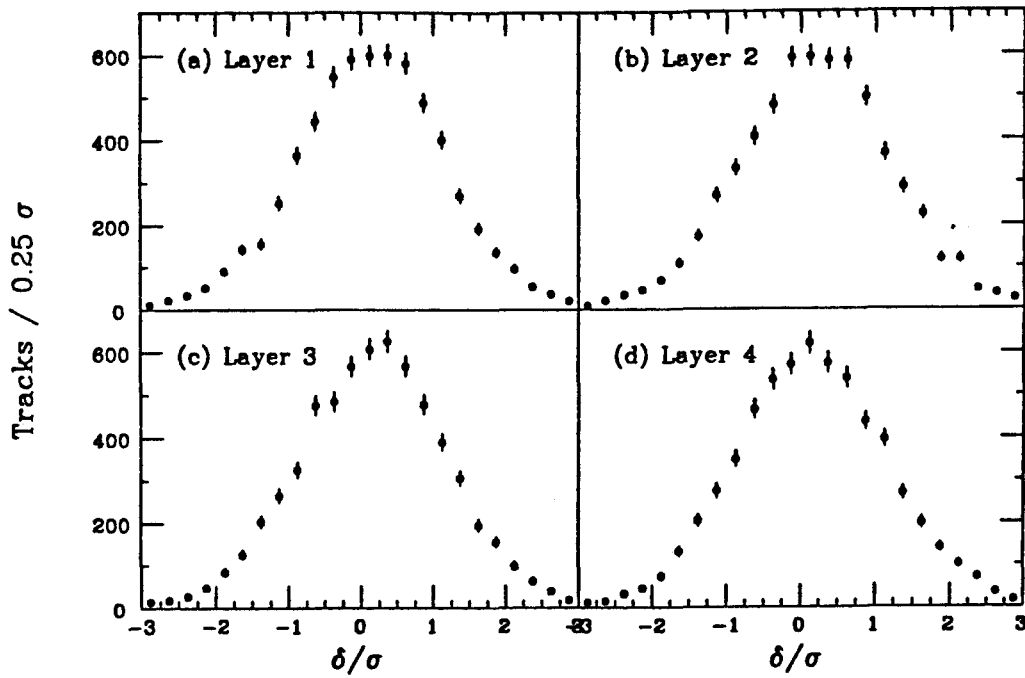


Figure 8: The distance between the track extrapolation and the nearest muon-chamber hit, δ , divided by σ for cosmic-ray muons. The values of σ_{res} used to calculate σ are listed in Table 5.

The values of σ_{res} for each layer and chamber orientation were adjusted to produce an rms hit-to-track distance of 1σ . The resulting σ_{res} obtained from a fit of the peak position and width of a Gaussian to the hit-distance distributions of Figure 8 are listed in Table 5. The

Layer number	Chamber orientation	Measured coordinate	σ_{res} (cm)	Peak (σ)	Width (σ)
1	East/West	z	1.1	0.02	0.98
2	East/West	y	1.4	0.68	1.02
3	East/West	y	1.4	0.53	1.00
4	East/West	y	1.7	0.46	1.00
1	Top/Bottom	z	0.9	0.14	0.98
2	Top/Bottom	x	0.8	0.23	0.99
3	Top/Bottom	x	0.8	0.15	0.98
4	Top/Bottom	x	0.9	0.13	0.99

Table 5: The values for σ_{res} in each layer for the fits that give unit-width Gaussians in the cosmic-ray hit-distance distributions (Figure 8).

offsets of about $+\sigma/2$ in the peak position of the y -coordinate measurements are the same for the chambers in both the East and the West walls. The effect of these offsets on the muon identification efficiency is small for the large (3σ) search width used here.

The search width around the DC track extrapolation in the outer layer can be quite large for tracks with small momenta. Empirically, for $p < 10 \text{ GeV}/c$, $\sigma \simeq 20/p(\text{GeV}/c) \text{ cm}$ in the fourth layer. To better reject noise hits in the outer layer, which is important in the noisy SLC environment, we use a smaller search region about the path defined by the associated hits in the second and third layers, thus demanding that the hits in the outer layers be correlated [Weir 88]. This search region is $3\sigma_{\text{corr}}$, where σ_{corr} , the rms deviation of hits in the fourth layer from this path, is typically 1 to 3 cm.

We determine σ_{corr} from cosmic-ray tracks recorded with the Mark II at the SLC, and the result agrees well with muon-pair events recorded at PEP. The rms deviation is parameterized as

$$\sigma_{\text{corr}} = \frac{1.47 + 0.74p_{\text{ext}}^{-1.78}}{\cos^{2.68}(\psi)} \text{ cm}, \quad (4)$$

where p_{ext} is the geometric mean of the extrapolated momenta at layers 3 and 4 in GeV/c , and where ψ is the angle in radians, between the track extrapolation and the normal of layer 4, projected onto the plane perpendicular to the orientation of the proportional tubes.

The deviations, divided by σ_{corr} , are shown for cosmic rays in Figure 9. Part of the non-Gaussian tails are due to tracks with multiple hits in a layer.

A track is identified as a muon if hits are found in all four layers of the muon system within 3σ of the extrapolated DC track and if the associated hit in the fourth layer is within

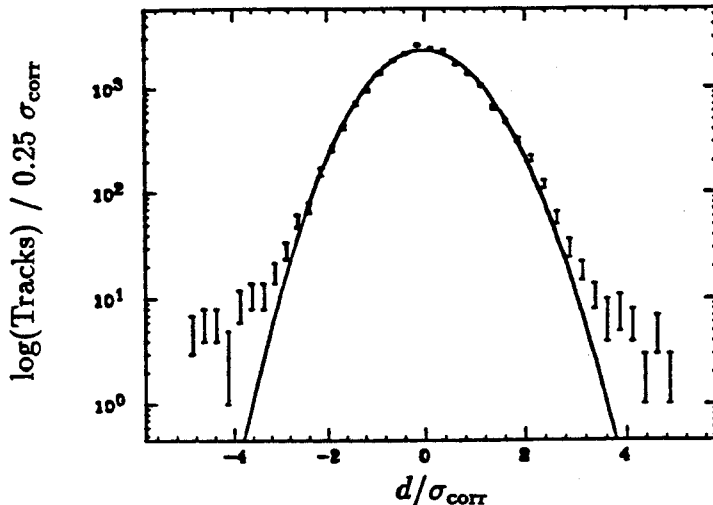


Figure 9: The deviation between the path defined by the associated hits in layers 2 and 3 and the associated hit in layer 4, d , divided by σ_{corr} for cosmic-ray muons. The solid line is a unit-width Gaussian [Weir 88].

$3\sigma_{\text{corr}}$ of the path defined by the second and third layers. In the following sections, we estimate the identification efficiencies and punch-through probabilities using the variable MUSTAT which contains a bit pattern of the layers which have associated hits within 3σ of the DC extrapolation. The bits are ordered such that the least significant bit corresponds to the first layer. That is, tracks with a hit in only the first layer have $\text{MUSTAT} = 1 = 0001_2$, tracks with hits in the first three layers have $\text{MUSTAT} = 7 = 0111_2$, and muon candidates are required to have $\text{MUSTAT} = 15 = 1111_2$. In addition, muon candidates need to have a correlated hit in layer four, described by defining the variable $\text{MUSTAT}_{\text{cr}}$, whose most significant bit also reflects this additional requirement. The values of the variable $\text{MUSTAT}_{\text{cr}}$ are the same as those of MUSTAT when $\text{MUSTAT} < 8$. For $\text{MUSTAT}_{\text{cr}}$ to be ≥ 8 , the fourth hit has to be both within 3σ and within $3\sigma_{\text{corr}}$. Thus, identified muons satisfy $\text{MUSTAT}_{\text{cr}} = 15$.

3.3 Muon Identification Efficiency

The majority of tracks in hadronic events fail muon identification by failing the muon-system fiducial criteria, that the DC track extrapolation be contained within the edges of the fourth layer and that the track momentum be sufficient to penetrate to the fourth layer. The minimum momentum for tracks at normal incidence to the absorbers is about $1.8 \text{ GeV}/c$. These criteria are well-simulated in the Monte Carlo: the fraction of reconstructed tracks** with $p > 2 \text{ GeV}/c$ which are inside the muon fiducial volume is 0.429 ± 0.002 in the MC and 0.42 ± 0.01 in the data.

Muons that satisfy the fiducial criteria can fail to be identified if they scatter out of the

**Reconstructed tracks satisfy $|\cos \theta| < 0.85$.

Layer number	$\mu^+\mu^-$ MC			Cosmic-ray data		
	One missing	Ineff'cy	Efficiency	One missing	Ineff'cy	Efficiency
1	0.020	0.020	0.980	0.036	0.040	0.960
2	0.009	0.009	0.991	0.042	0.048	0.952
3	0.005	0.006	0.994	0.036	0.040	0.960
4	0.016	0.016	0.984	0.032	0.037	0.963
Ave/Tot		0.013	0.950		0.041	0.845

Table 6: Calculation of muon-chamber efficiencies in each layer for tracks from simulated muon pairs and observed cosmic rays with $32 < p < 64$ GeV/ c . The inefficiency for a layer is defined as the number of tracks with the given layer missing (including tracks missing multiple hits) divided by the total number of tracks. It is obtained by iteration from the ratio labelled ‘One missing,’ which is defined as the number of tracks with exactly one hit missing in the given layer (i.e. with MUSTAT = 14, 13, 11 or 7) divided by the total number of tracks.

active volume or the 3σ search region in some layer, if they fail to penetrate to the outer layer because of larger-than-average dE/dx losses, if their trajectory is poorly reconstructed in the DC, or if the proportional tubes fail to fire due to electronic inefficiencies. All of these effects are incorporated in the Monte Carlo simulation. However, the proportional-tube inefficiency was set to 1% per layer in the MC, significantly smaller than the $3\% \pm 1\%$ measured with muon-pair events at PEP [Nelson 83b].

We estimate the difference in efficiencies between the data and the MC by counting the number of tracks failing in only one layer, tracks with MUSTAT = 14, 13, 11 or 7. In Table 6, we calculate the efficiencies in each layer for MC Z decays to muon pairs and for energetic cosmic rays recorded at the SLC. The average per-layer inefficiency is 0.013 ± 0.007 in the MC and 0.041 ± 0.004 in the cosmic-ray data. To account for this difference, we add the inefficiency $\epsilon_{\text{add}} = 0.029 \pm 0.008$ per layer to the MC, thereby reducing the simulated muon identification efficiency by the factor $(0.845 \pm 0.014)/(0.950 \pm 0.027) = 0.89 \pm 0.03$.

The efficiency for identifying isolated muon tracks that satisfy the muon-system fiducial criteria in hadronic events is 0.79 ± 0.05 , as calculated from the corrected numbers of isolated MC muon tracks in Table 7.

3.4 Muon Misidentification Probability

Misidentification in the muon sample comes from track overlap, noise hits and hadron punch through. The data also contain muons from hadron decay in flight; these muons are realistically simulated in the Monte Carlo [Nelson 83b] and are part of the sample of real muons, as a background to prompt muons from heavy-quark decay. Beam-induced noise

Particle	Webber-Marchesini	Lund	Both models
Muon	238.3/297 = 0.802	207.1/266 = 0.779	445.4/563 = 0.791 ± 0.013
Non-muon	49.1/7917 = 0.0062	42.1/6328 = 0.0067	91.2/14245 = 0.0064 ± 0.0007

Table 7: Corrected numbers of isolated muon and non-muon tracks identified as muons in the Monte Carlo. The corrections, for the additional proportional-tube inefficiencies calculated in Section 0.3.3 (on page 16), and for the additional hadron punch-through probabilities outlined in Section 0.3.4 (on pages 17–18), are described in detail in Appendix A. The denominators are the numbers of tracks with $p > 2$ GeV/ c and $p_t > 1.25$ GeV/ c which satisfy the muon-system fiducial criteria, and the numerators are the subsets of these tracks which satisfy $MUSTAT_{cr} = 15$. The uncorrected ratios are $501/563 = 0.890 \pm 0.014$ for MC muons and $91/14245 = 0.0064 \pm 0.0007$ for MC non-muons. MC muons from hadron decay in flight are categorized as real muons.

hits are simulated well by mixing the signals from each MC event with the signals from a background event: the fraction of tracks inside the muon fiducial volume with an associated hit in the fourth layer, i.e. with $MUSTAT > 7$, is 0.233 ± 0.001 in the MC and 0.23 ± 0.01 in the data. The simulation of hadron punch through is only good to a factor of two, as was learned from studies with a detailed hadronic interaction simulation (FLUKA87) [Aarnio 86, Ranft 86, Nelson 85], which was found to describe well hadrons in hadronic events recorded with the Mark II detector at PEP [Weir 87].

Using tracks in the data which penetrate to the inner three layers of the muon system, we determine the additional hadron punch-through probabilities to these layers, thus correcting the MC $MUSTAT$ distribution. Table 8 lists the probabilities for tracks to reach each layer. The differences between the probabilities in the middle two columns (2 and 3) of Table 8 indicate that the punch through to the first three layers is underestimated in the MC by about a factor two. To calculate the effect of this underestimate on the punch through reaching the $MUSTAT = 15$ signal population, we fit the MC $MUSTAT < 15$ distribution to the data, resulting in the higher probabilities listed in the last column (4) of Table 8. The corrections, for the additional hadron punch-through probabilities outlined here and for the additional proportional-tube inefficiencies calculated in the previous section (on page 16), to the numbers of identified muons predicted by the Monte Carlo are described in detail in Appendix A.

To estimate the number of isolated hadrons misidentified as muons, we correct the numbers of such tracks in the MC by using the probabilities for additional hadrons to punch through to layers 1 to 3 obtained from a fit to the distribution of the non-signal values of the muon identification variable ($MUSTAT_{cr} = 0-14$) for all tracks^{††} as well as the additional

^{††}To determine the additional inner-layer punch-through probabilities, we use a fit to $MUSTAT_{cr}$ for *all* tracks instead of the subset of *isolated* tracks, in order to enhance the statistics for the fit. Within our

Layer number	Probability per track		
	Data	MC	MC fit
1	0.174 ± 0.013	0.118 ± 0.001	0.187 ± 0.001
2	0.064 ± 0.009	0.039 ± 0.001	0.066 ± 0.001
3	0.023 ± 0.006	0.011 ± 0.000	0.025 ± 0.001
4	0.028 ± 0.006	0.026 ± 0.001	0.029 ± 0.001

Table 8: Probabilities for tracks to reach each layer of the muon system in the data, the uncorrected MC and the corrected MC. The probabilities are calculated by dividing the numbers of tracks which leave hits (within 3σ) in all layers preceding and including the given layer but not in subsequent layers (i.e. tracks with $MUSTAT = 1, 3, 7$ or 15) by the total numbers of $p > 2$ GeV/ c tracks satisfying the muon fiducial criteria. The majority of tracks reaching the fourth layer are real muons.

proportional-tube inefficiencies. The probability for isolated hadrons to punch through to layer 4 is consistent with the probabilities obtained from a detailed study with the full FLUKA87 simulation [Weir 87]. Figure 10 is a comparison between $MUSTAT_{cr}$ for isolated tracks in the data and in the corrected MC, indicating the predicted contribution from real muons.

The probability for isolated non-muon tracks to be misidentified as muons is $0.006^{+0.006}_{-0.003}$, as calculated from the corrected numbers of isolated MC non-muon tracks in Table 7. This probability does not include muons from π or K decays in flight, which are categorized as real muons.

The p_t spectrum for tracks identified as muons is shown in Figure 11, together with predictions for the contributions from real muons and hadrons misidentified as muons. There are 6 isolated tracks identified as muons in the data. Of these 6 tracks, 0.9 are expected to come from hadrons misidentified as muons. Figure 12 is a picture of an event with an isolated muon.

4. Acknowledgements

Thanks to all the Mark II physicists involved in lepton identification throughout the years. The whole Caltech group deserves thanks for making lepton identification with the LA and muon systems possible at the SLC. Thanks to George Trilling for supervising my work.

limited statistics, insignificant differences in the estimated misidentification probability for isolated tracks result from using the additional punch-through probabilities obtained from fits to either $MUSTAT$ or $MUSTAT_{cr}$ and from using either all tracks or only isolated tracks. See Appendix A for details.

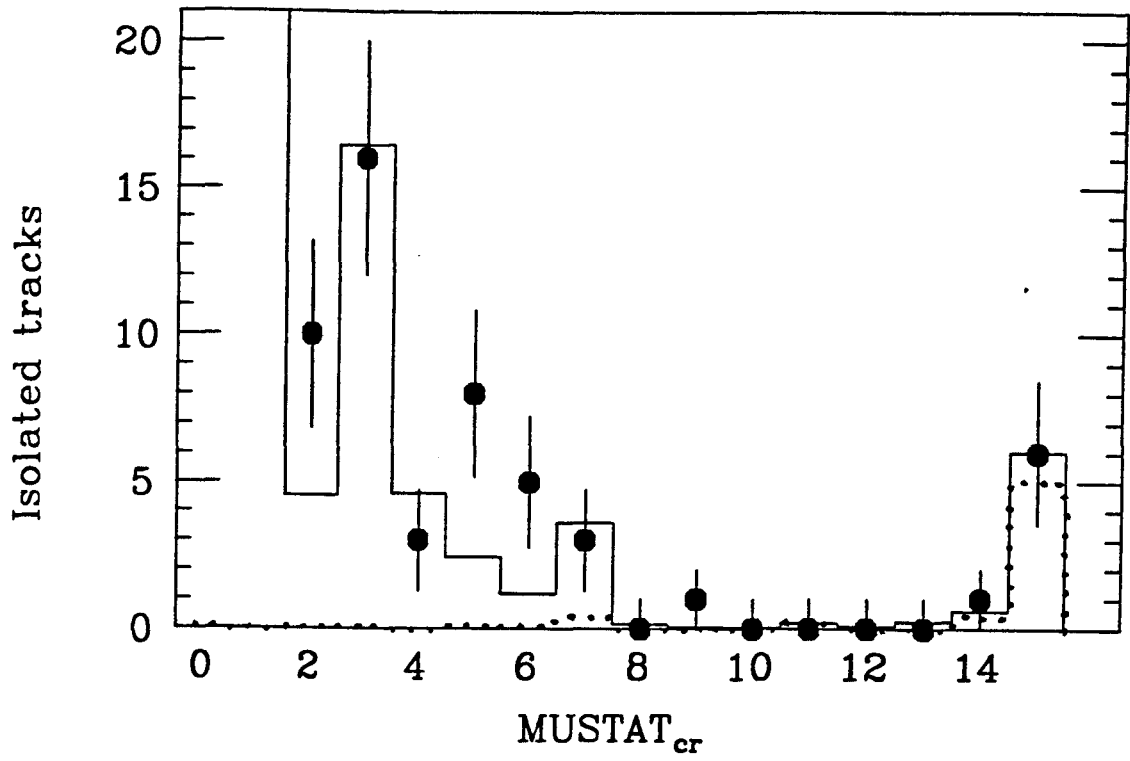


Figure 10: Comparison of muon identification variable in the data (circles) and the corrected MC (solid) for isolated tracks. The dotted histogram is the prediction for real muons. Identified muons have $MUSTAT_{cr} = 15$.

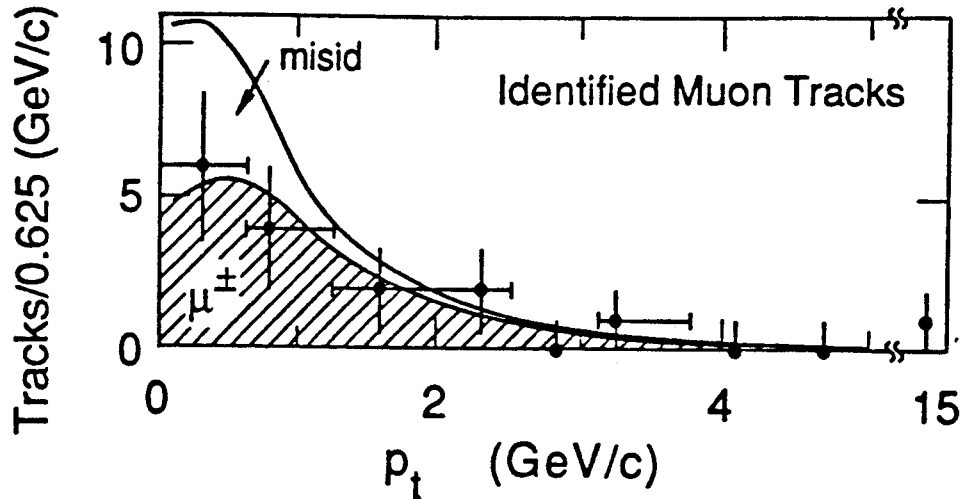


Figure 11: The p_t spectrum for tracks identified as muons. The shaded and unshaded regions show the uncorrected expected contributions from real muons and hadrons misidentified as muons, respectively. The predictions come from MC simulations normalized to 413 observed hadronic events, assuming $r_b = 0.22$. The numbers of identified muons have not been corrected for additional inefficiencies or punch through. The net effect of these corrections, evaluated in the footnote on page 25 in Appendix A, is to multiply the numbers of real muons and hadrons identified as muons by the relatively small overall factors of $(1 - \epsilon_{\text{add}})^4 = 0.89$ and $652.2/616 = 1.06$, respectively. The reasons for the disagreement between MC and data for tracks with small values of p_t are not understood. For isolated non-muon tracks identified as muons, i.e. misidentified hadrons with $p_t > 1.25$ GeV/c, the overall correction factor is $91.2/91 = 1.00$, as shown in Table 7.

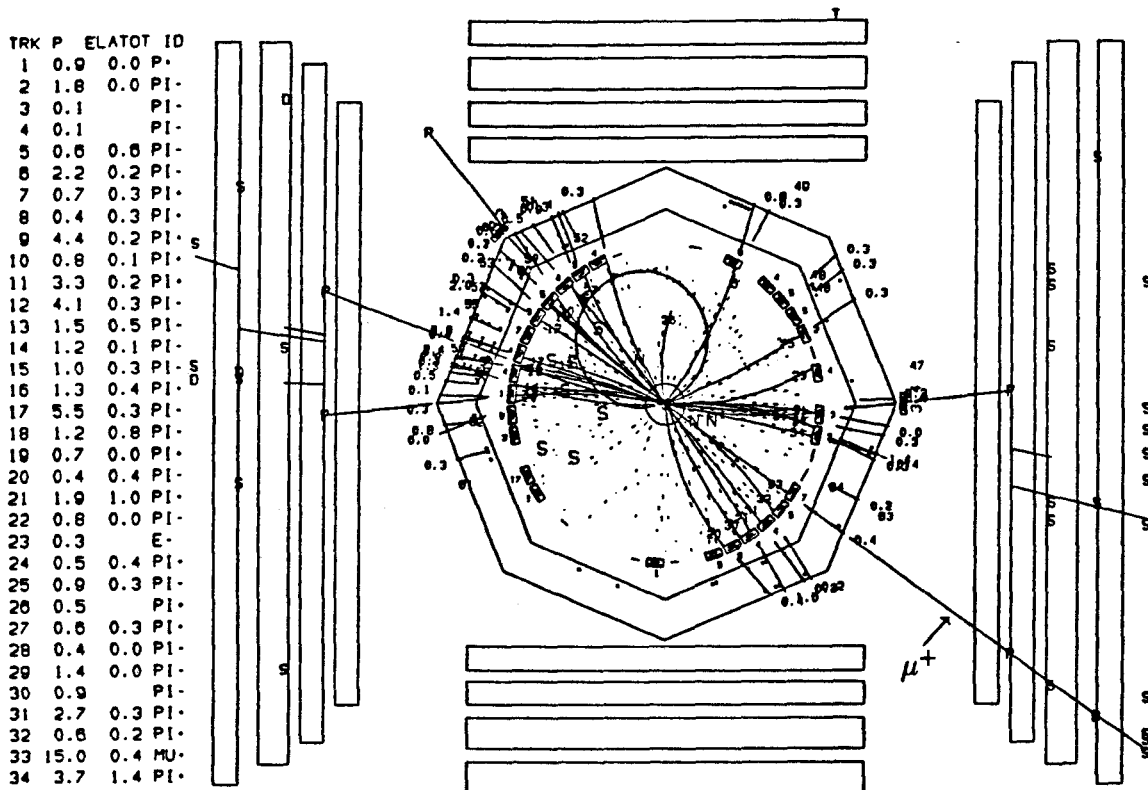


Figure 12: Hadronic Z -decay event with an isolated muon shown with charged tracks, neutral showers and muon-chamber hits in the r - ϕ plane. Track number 33 has $p = 15.7$ GeV/ c , $p_t = 2.2$ GeV/ c , all four associated hits $< 1.3\sigma$ from the DC track extrapolation and a fourth-layer hit at $-1.2\sigma_{\text{corr}}$ from the path defined by the associated hits in layers 2 and 3.

Appendix A

Muon Monte Carlo Corrections

To estimate the muon misidentification probability in Section 3, we use data to correct the muon Monte Carlo simulation for additional hadron punch-through probabilities and additional proportional-tube inefficiencies. We obtain the corrected punch-through probabilities for the inner three layers from a fit to the distribution of hits for tracks which do not reach the outer layer [Nelson 83b]. The distribution of hits is then corrected for the measured tube inefficiency. The correction procedure outlined in Section 0.3.4 is described in detail here.

The pattern of hits in the four layers of the muon system for each track is represented in the binary variable MUSTAT, for which the least significant bit represents the first layer. E.g., a track penetrating to the third layer without reaching the fourth has $\text{MUSTAT} = 0111_2 = 7$. The values of the variable $\text{MUSTAT}_{\text{cr}}$ are the same as those of MUSTAT when $\text{MUSTAT} < 8$. For $\text{MUSTAT}_{\text{cr}}$ to be ≥ 8 , the fourth hit has to be both within 3σ and within $3\sigma_{\text{corr}}$. Hence, identified muons have $\text{MUSTAT}_{\text{cr}} = 1111_2 = 15$.

The probabilities $P_{\text{add}}^{(i)}$ measure how much extra punch through we need to add to each of the inner three layers, $i = 1-3$. Using the fraction $P_{\text{add}}^{(i)}$ of the tracks with a given value of MUSTAT, we perform the logical operation $\text{MUSTAT OR MASK}^{(i)}$, where $\text{MASK}^{(1)} = 0001_2$, $\text{MASK}^{(2)} = 0011_2$ and $\text{MASK}^{(3)} = 0111_2$. Thus, $P_{\text{add}}^{(1)}$ of the tracks with $\text{MUSTAT} = 0$ change to $\text{MUSTAT} = 1$, since $0000_2 \text{ OR } 0001_2 = 0001_2$. Similarly, $P_{\text{add}}^{(1)}$ of the tracks with $\text{MUSTAT} = 2$ change to $\text{MUSTAT} = 3$, since $0010_2 \text{ OR } 0001_2 = 0011_2$, whereas the tracks with $\text{MUSTAT} = 1$ do not change, since they already contain a hit in the first layer. Starting with k_j tracks having

MUSTAT = j , we end up with l_j tracks,

$$\begin{aligned}
l_0 &= [1 - P_{\text{add}}^{(1)} - P_{\text{add}}^{(2)} - P_{\text{add}}^{(3)}]k_0 \\
l_1 &= P_{\text{add}}^{(1)}k_0 + [1 - P_{\text{add}}^{(2)} - P_{\text{add}}^{(3)}]k_1 \\
l_2 &= [1 - P_{\text{add}}^{(1)} - P_{\text{add}}^{(2)} - P_{\text{add}}^{(3)}]k_2 \\
l_3 &= P_{\text{add}}^{(1)}k_2 + P_{\text{add}}^{(2)}[k_0 + k_1 + k_2] + [1 - P_{\text{add}}^{(3)}]k_3 \\
l_4 &= [1 - P_{\text{add}}^{(1)} - P_{\text{add}}^{(2)} - P_{\text{add}}^{(3)}]k_4 \\
l_5 &= P_{\text{add}}^{(1)}k_4 + [1 - P_{\text{add}}^{(2)} - P_{\text{add}}^{(3)}]k_5 \\
l_6 &= [1 - P_{\text{add}}^{(1)} - P_{\text{add}}^{(2)} - P_{\text{add}}^{(3)}]k_6 \\
l_7 &= P_{\text{add}}^{(1)}k_6 + P_{\text{add}}^{(2)}[k_4 + k_5 + k_6] + P_{\text{add}}^{(3)}[k_0 + k_1 + k_2 + k_3 + k_4 + k_5 + k_6] \\
&\dots \\
l_{15} &= P_{\text{add}}^{(1)}k_{14} + P_{\text{add}}^{(2)}[k_{12} + k_{13} + k_{14}] \\
&\quad + P_{\text{add}}^{(3)}[k_8 + k_9 + k_{10} + k_{11} + k_{12} + k_{13} + k_{14}].
\end{aligned} \tag{1}$$

Then we apply the layer inefficiency $\epsilon_{\text{add}} = 0.029$, as calculated in Table 6, to each of these MUSTAT populations, obtaining the corrected populations m_j for each MUSTAT value $j = 0-15$,

$$\begin{aligned}
m_0 &= l_0 + \epsilon_{\text{add}}(l_1 + l_2 + l_4 + l_8) + \epsilon_{\text{add}}^2(l_3 + l_5 + l_6 + l_9 + l_{10} + l_{12}) \\
&\quad + \epsilon_{\text{add}}^3(l_7 + l_{11} + l_{13} + l_{14}) + \epsilon_{\text{add}}^4 l_{15} \\
m_1 &= (1 - \epsilon_{\text{add}})[l_1 + \epsilon_{\text{add}}(l_3 + l_5 + l_9) + \epsilon_{\text{add}}^2(l_7 + l_{11} + l_{13}) + \epsilon_{\text{add}}^3 l_{15}] \\
m_2 &= (1 - \epsilon_{\text{add}})[l_2 + \epsilon_{\text{add}}(l_3 + l_6 + l_{10}) + \epsilon_{\text{add}}^2(l_7 + l_{11} + l_{14}) + \epsilon_{\text{add}}^3 l_{15}] \\
m_3 &= (1 - \epsilon_{\text{add}})^2[l_3 + \epsilon_{\text{add}}(l_7 + l_{11}) + \epsilon_{\text{add}}^2 l_{15}] \\
&\dots \\
m_{15} &= (1 - \epsilon_{\text{add}})^4 l_{15}.
\end{aligned} \tag{2}$$

To determine the probabilities $P_{\text{add}}^{(i)}$, we perform a fit to the observed MUSTAT distribution, excluding the MUSTAT = 15 population since it consists mostly of real muons. For each of the 15 remaining values of MUSTAT = 0-14, we form the Poisson probability,

$$P_j = \frac{r_j^{n_j} e^{-r_j}}{n_j!}, \tag{3}$$

corresponding to the Poisson probability of observing n_j tracks with $j = \text{MUSTAT}$, when r_j are predicted. The predictions are the corrected MC populations normalized to the total number of tracks, $r_j = \frac{\sum_{j=0}^{15} n_j}{\sum_{j=0}^{15} m_j} m_j$. We maximize the likelihood

$$\mathcal{L} = \prod_{j=0}^{14} P_j, \tag{4}$$

which implicitly depends on the punch-through probabilities $P_{\text{add}}^{(i)}$ through the number of predicted tracks r_j . The fit is performed by minimizing $-\log \mathcal{L}$ using the computer program

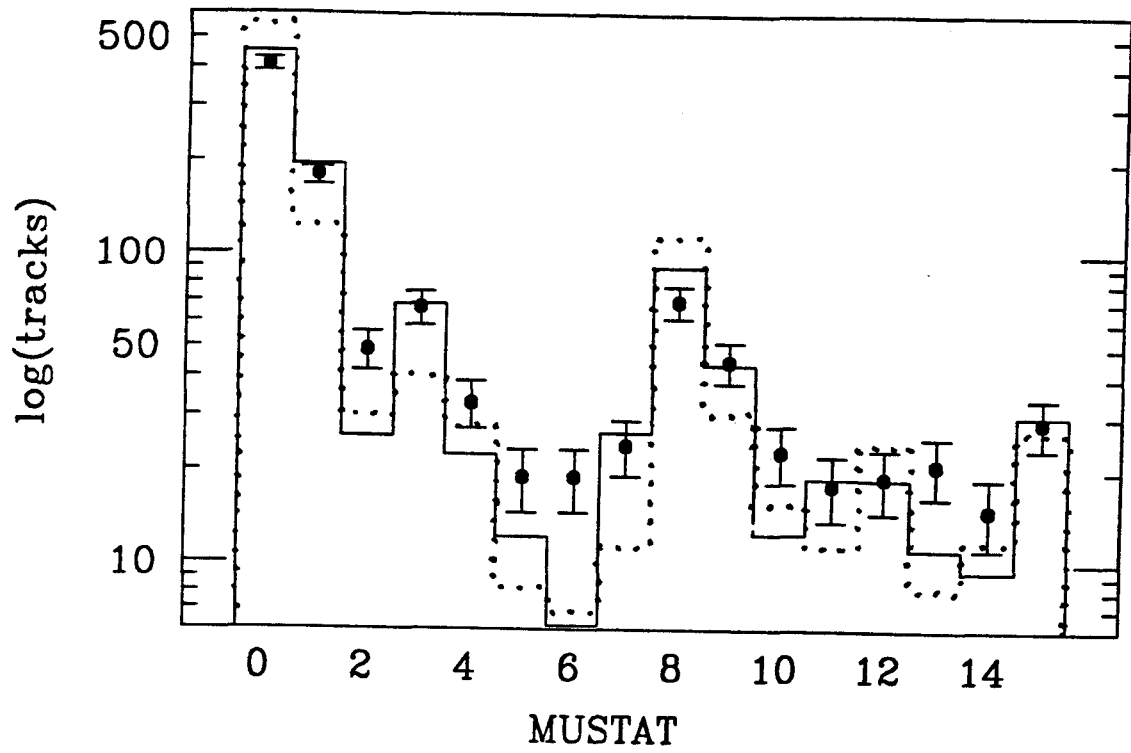


Figure A.1: Result of fit for hadron punch through to pattern of muon hits. Shown are the MUSTAT distributions for tracks satisfying the muon fiducial criteria in the Monte Carlo, before (dots) and after (solid) the corrections, and in the data (circles).

MINUIT [James 75]. The observed MUSTAT distribution for all tracks is compared to the simulated distributions before and after the fit in Figure A.1. To make sure that the fit yields consistent results, we also fit $P_{\text{add}}^{(i)}$ to the distributions of MUSTAT_{cr} using all tracks and using only isolated tracks and the results are given in Table A.1.

Fit results	MUSTAT	MUSTAT _{cr}	
	all	all	isolated
$P_{\text{add}}^{(1)}$	0.147 ± 0.020	0.147 ± 0.020	0.162 ± 0.047
$P_{\text{add}}^{(2)}$	0.039 ± 0.011	0.039 ± 0.011	0.045 ± 0.030
$P_{\text{add}}^{(3)}$	0.018 ± 0.007	0.021 ± 0.007	0.003 ± 0.030

Table A.1: Additional punch-through probabilities obtained from fits to MUSTAT and MUSTAT_{cr} for all tracks and to MUSTAT_{cr} for the subset of isolated tracks.

To calculate the muon misidentification probability for isolated tracks, we correct the MUSTAT_{cr} distribution for these tracks using the additional punch-through probabilities obtained from the fit to MUSTAT_{cr} for the larger sample containing all tracks,* $P_{\text{add}}^{(1)} = 0.147$, $P_{\text{add}}^{(2)} = 0.039$ and $P_{\text{add}}^{(3)} = 0.021$. Table A.2 shows the corrections to the MC for each MUSTAT_{cr} bin. The resulting MUSTAT_{cr} distribution, indicating the contribution from real muons, is compared with the observed distribution in Figure 10.

Out of the 563 isolated real muons in the MC, 501 are identified as muons. The inefficiency correction changes the number of identified muons to 445.4, leading to the identification efficiency of 0.79, as quoted in Section 0.3.3. Similarly, out of the 14245 isolated non-muons in the MC, 91 are misidentified as muons. The punch-through correction adds 11.6 non-muon tracks while the inefficiency corrections subtracts 11.4 non-muon tracks, yielding the essentially unchanged number of 91.2 tracks misidentified as muons and the misidentification probability of 0.006, as quoted in Section 0.3.4. The change in the misidentification probability when results from the other fits in Table A.1 are used is insignificant.

*This fit is to 1419 real muons and 616 hadrons identified as muons in the MC. The number of tracks from additional punch through is +117.7 hadrons and the numbers of tracks from additional inefficiencies are -157.6 muons and -81.5 hadrons. The net effect of these corrections is to multiply the numbers of real muons and hadrons by the overall factors of $(1 - \epsilon_{\text{add}})^4 = 0.89$ and $652.2/616 = 1.06$, respectively, as is suggested for the uncorrected p_t spectrum of Figure 11. The overall correction factor is equal to unity for misidentified isolated hadrons, as is shown here.

j	Before	Punch.	Ineff.	After	r_j	n_j
0	9882	-2045.6	+117.0	7953.4	89.7	82
1	1848	+1341.8	-45.2	3144.5	35.5	32
2	464	-96.0	+33.4	401.4	4.5	10
3	923	+524.4	-66.6	1380.8	15.6	16
4	518	-107.2	-2.6	408.2	4.6	3
5	141	+67.7	+4.3	213.0	2.4	8
6	125	-25.9	+11.5	110.6	1.2	5
7	230	+340.9	-32.2	538.7	6.1	3
8	17	-3.5	+0.0	13.5	0.2	0
9	3	+2.3	+0.4	5.7	0.1	1
10	2	-0.4	+1.5	3.1	0.0	0
11	1	+1.1	+15.8	18.0	0.2	0
12	7	-1.4	+1.4	7.0	0.1	0
13	5	+0.7	+15.5	21.3	0.2	0
14	50	-10.4	+12.7	52.3	0.6	1
15	592	+11.6	-67.0	536.5	6.1	6
\sum_j	14808	0.0	0.0	14808.0	167.0	167.0

Table A.2: The Monte Carlo $MUSTAT_{cr}$ distributions for isolated tracks before and after corrections for punch through and inefficiency. The predicted total numbers of tracks r_j are compared to the observed numbers of tracks n_j for each value of $j = MUSTAT_{cr}$.

Bibliography

- [Aarnio 86] P. A. Aarnio *et al.*, CERN-TIS-RP/168, January 1986 (unpublished).
- [Andersson 83] B. Andersson *et al.*, Phys. Rep. **97**, 31 (1983).
- [Bengtsson 87] M. Bengtsson and T. Sjöstrand, Nucl. Phys. **B289**, 810 (1987).
- [Gan 87] K. K. Gan, Mark II/SLC Note #195, December 1987 (unpublished).
- [James 75] F. James and M. Roos, Comput. Phys. Commun. **10**, 343 (1975).
- [James 80] F. James and M. Roos, Nucl. Phys. **B172**, 475 (1980),
- [Kral 89a] J. F. Kral, Mark II/SLC Note #24x, October 24, 1989 (unofficial).
- [Kral 89b] J. F. Kral, Mark II/SLC Note #24y, October 27, 1989 (unofficial).
- [Kral 90a] J. F. Kral *et al.*, Phys. Rev. Lett. **64**, 1211 (1990).
- [Kral 90b] J. F. Kral, LBL-29485, Ph.D. Thesis, September 1990 (unpublished).
- [Kral 90c] J. F. Kral, Mark II/SLC Note #249, October 1990 (unpublished).
- [Lamport 86] L. Lamport, *L^AT_EX: A Document Preparation System* (Addison-Wesley, Menlo Park, California, 1986).
- [Marchesini 84] G. Marchesini and B. R. Webber, Nucl. Phys. **B238**, 1 (1984).
- [Nelson 83a] M. E. Nelson *et al.*, Phys. Rev. Lett. **50**, 1542 (1983).
- [Nelson 83b] M. E. Nelson, LBL-16724, Ph.D. Thesis, October 1983 (unpublished).
- [Nelson 85] W. R. Nelson *et al.*, SLAC-265, December 1985 (unpublished).
- [Ong 87] R. A. Ong, SLAC-320, Ph.D. Thesis, September 1987 (unpublished).
- [Ong 88] R. A. Ong *et al.*, Phys. Rev. Lett. **60**, 2587 (1988).
- [Petersen 88] A. Petersen *et al.*, Phys. Rev. D **37**, 1 (1988).
- [Ranft 86] J. Ranft *et al.*, SLAC-TN-86-3, April 1986 (unpublished).

- [Rossi 52] B. Rossi, *High-Energy Particles*, (Prentice-Hall, New York, 1952), pp. 66–69.
- [Sjöstrand 83] T. Sjöstrand, *Comput. Phys. Commun.* **28**, 229 (1983).
- [Sjöstrand 86] T. Sjöstrand, *Comput. Phys. Commun.* **39**, 347 (1986).
- [Sjöstrand 87] T. Sjöstrand and M. Bengtsson, *Comput. Phys. Commun.* **43**, 367 (1987).
- [Webber 84] B. R. Webber, *Nucl. Phys.* **B238**, 492 (1984).
- [Weir 87] A. J. Weir, Mark II/SLC Note #193, December 1987 (unpublished).
- [Weir 88] A. J. Weir, Mark II/SLC Note #213, May 1988 (unpublished).